LETTERS
PUBLISHED ONLINE: 18 OCTOBER 2009 | DOI: 10.1038/NPHOTON.2009.187
nature photonics

Large single-molecule fluorescence enhancements produced by a bowtie nanoantenna

Anika Kinkhabwala[1], Zongfu Yu[2], Shanhui Fan[2], Yuri Avlasevich[3], Klaus Müllen[3] and W. E. Moerner[1]*

Owing to the size mismatch between light and nanoscale objects such as single molecules, it is important to be able to control light–molecule interactions[1–4]. Plasmonic nanoantennas create highly enhanced local fields when pumped resonantly, leading to increased Raman scattering[5], but whether fluorescence enhancement occurs depends upon a variety of factors. Although sharp metal tips[6] and colloids[7,8] can enhance fluorescence, the highly enhanced optical fields of lithographically fabricated bowtie nanoantennas[9] provide a structure that is more controllable and amenable to integration. Using gold bowties, we observe enhancements of a single molecule's fluorescence up to a factor of 1,340, ten times higher than reported previously[7,8,10–22]. Electromagnetic simulations reveal that this is a result of greatly enhanced absorption and an increased radiative emission rate, leading to enhancement of the intrinsic quantum efficiency by an estimated factor of nine, despite additional non-radiative ohmic effects. Bowtie nanoantennas thus show great potential for high-contrast selection of single nanoemitters.

A single fluorescent molecule (SM) with transition dipole $\boldsymbol{\mu}$ acts as a nanoscale optical sensor of the local field $\mathbf{E}$ near a bowtie nanoantenna because its transition rate is proportional to $|\boldsymbol{\mu} \cdot \mathbf{E}|^2$, and its emission can either couple to the far field via the nanoantenna or quench through ohmic losses[23,24]. Low-quantum-efficiency emitters have been noted to have much higher potential fluorescence brightness enhancements (f_F) than high-quantum-efficiency emitters, because their intrinsic quantum efficiency has a greater potential to be improved by the presence of the antenna[25,26].

Experimental measurements of f_F for a SM were performed by coating electron-beam-fabricated gold bowtie nanoantennas with a relatively low fluorescence quantum efficiency of $\eta_0 \approx 2.5\%$ but solubilized near-infrared (NIR) dye *N*,*N*′-bis(2,6-diisopropylphenyl)-1,6,11,16-tetra-[4-(1,1,3,3-tetramethylbutyl)phenoxy]quaterylene-3,4:13,14-bis(dicarboximide) (TPQDI) doped in a thin poly(methyl methacrylate) (PMMA) layer (Fig. 1a). In addition to its low quantum efficiency, TPQDI (Fig. 1b) was chosen for the overlap of its absorption and emission spectra with the measured bowtie plasmon resonance (Fig. 1e).

A 780-nm diode laser was used to excite fluorescence from the TPQDI in a confocal microscope. Appropriate excitation and emission filters ensured that only TPQDI fluorescence reached the avalanche photodiode (APD) photon-counting silicon detector. Figure 2a shows a confocal fluorescence scan from a low TPQDI concentration in PMMA without bowtie nanoantennas. Essentially all fluorescent molecules irreversibly photobleach after a certain number of excitation cycles due to photodegradation (for example, photo-oxidation), so each spot in the image was observed until single-step digital photobleaching occurred (Fig. 2c) to ensure it corresponded to a single unenhanced TPQDI molecule. Each molecule's dipole moment is randomly

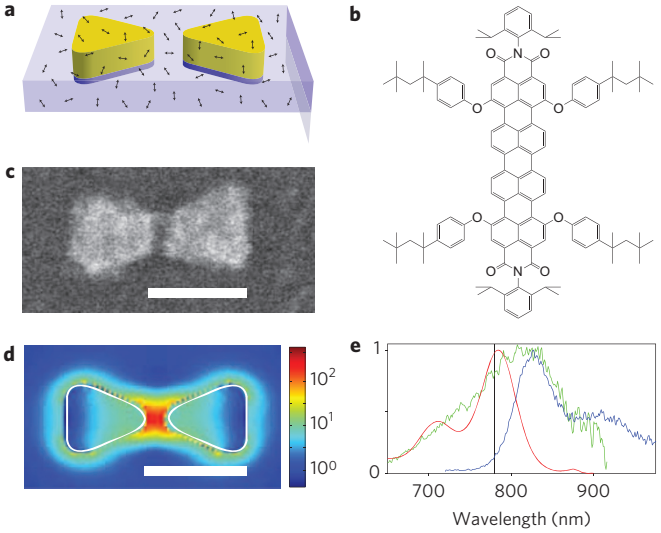

Figure 1 | Experimental set-up. a, Schematic of bowtie nanoantenna (gold) coated with TPQDI molecules (black arrows) in PMMA (light blue) on a transparent substrate. **b**, Molecular structure of TPQDI. **c**, Scanning electron microscopy (SEM) image of a gold bowtie nanoantenna. Scale bar, 100 nm. **d**, Finite-difference time-domain calculation of local intensity enhancement. Scale bar, 100 nm. **e**, Normalized absorption and emission spectra (red and blue traces, respectively) of TPQDI in toluene and scattering spectrum from the bowtie shown in **c** (green trace) measured as in ref. 30. The laser excitation wavelength is indicated by the black line.

oriented with respect to the linear excitation field polarization, so each spot has a different brightness, with the brightest spots arising from molecules with dipole moments aligned along the excitation polarization. To measure the brightness of an unenhanced molecule for which the dipole moment is oriented along the excitation field, $S_{un,max}$, 201 single molecules were measured and the intensities of the brightest five averaged (Supplementary Fig. S1), yielding 2.3 detected photons per 10 ms per μW excitation power.

Figure 2b shows a confocal scan from an array of 16 bowties coated with a high concentration of TPQDI in PMMA (~1,000 molecules/diffraction-limited spot or ~3 molecules/(10 nm)^2). To detect a SM among the many surrounding the bowtie, the fluorescence as a function of time is shown in Fig. 2d. Discrete blinking and eventual photobleaching of 50% of the total signal can be attributed to a single molecule's dynamics, revealing that half of the fluorescence from this particular bowtie is due to a single molecule! In other words, the digital (step-like) sudden drop near 293 s is an unambiguous signature that a single molecule photobleached, and the step size shows its contribution to the total signal, S_{bowtie}. Although the exact position and orientation of this molecule is

[1]Department of Chemistry Stanford University, Stanford, California 94305, USA, [2]Department of Electrical Engineering, Stanford University, Stanford, California 94305, USA, [3]Max-Planck Institute for Polymer Research, D-55128 Mainz, Germany. *e-mail: wmoerner@stanford.edu

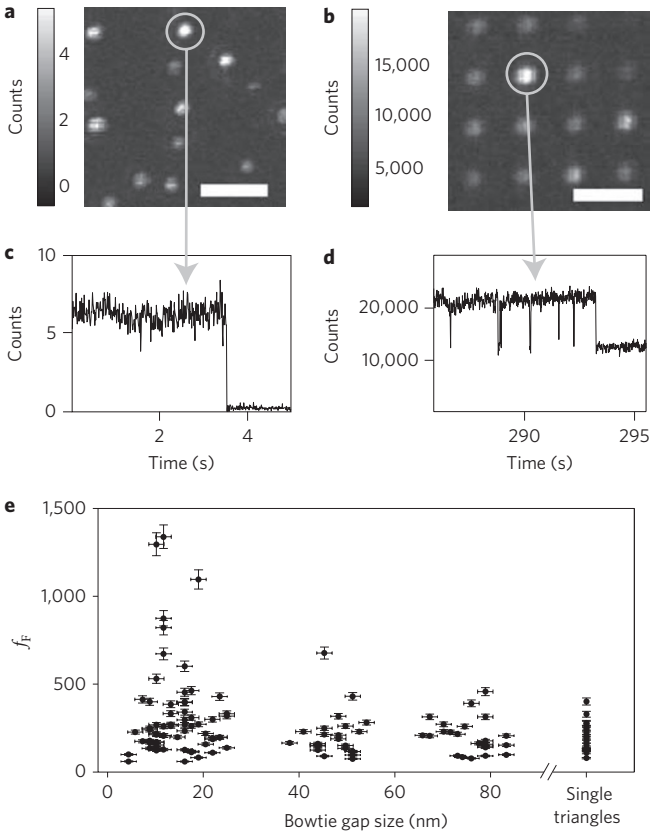

Figure 2 | Measurement of f_F for single fluorescent molecules (SMs) as a function of bowtie gap size. a, Confocal fluorescence scan of a low concentration (<1 molecule/diffraction-limited spot) sample of TPQDI in PMMA without bowtie nanoantennas. Scale bar, 4 μm. Data collected at 79 kW cm^{-2}, then scaled for direct comparison with **b. b**, Confocal scan of 16 bowties coated with a high concentration (~1,000 molecules/diffraction-limited spot) TPQDI in PMMA collected at 2.4 kW cm^{-2}. Scale bar, 4 μm. **c**, Fluorescence time trace of a single unenhanced TPQDI molecule aligned along the excitation polarization axis. **d**, Fluorescence time trace of the TPQDI/PMMA-coated bowtie nanoantenna shown in Fig. 1c. Blinking dynamics and eventual photobleaching are due to one molecule that has been enhanced by a factor of 1,340. **e**, Scatter plot of 129 SM fluorescence brightness enhancements, f_F, as a function of bowtie gap size. See Methods for an explanation of the error bars.

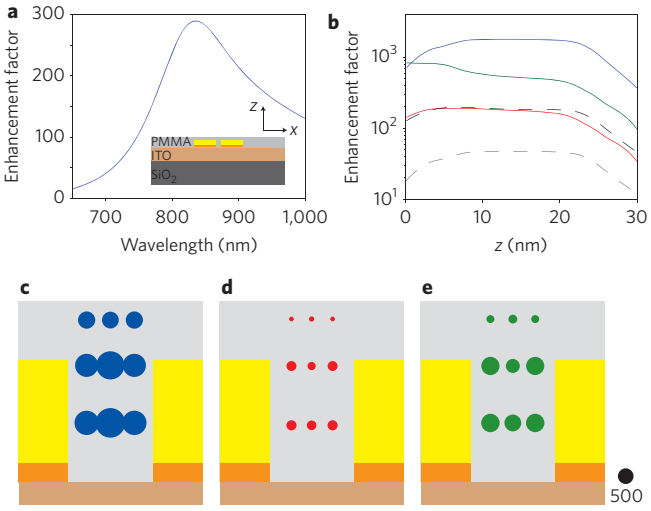

Figure 3 | Electromagnetic simulations of single fluorescent molecule fluorescence near a gold bowtie nanoantenna. a, Spectrum of calculated electric field intensity enhancement versus wavelength in the centre of a bowtie with a 14-nm gap. Inset: the simulated structure (side view) consists of a SiO_2 (refractive index $n = 1.47$) substrate, a 50-nm layer of indium tin oxide (ITO) ($n = 2$), and a 30-nm layer of PMMA ($n = 1.49$). The gold bowtie structure is 20 nm thick on a 4-nm layer of titanium. **b**, Radiative (red) and non-radiative (green) enhancement factors along the centre of the gap at a wavelength of 820 nm; z is a measure of the distance above the ITO/PMMA interface. The black dashed line represents the local optical intensity enhancement at 780 nm. The blue curve shows the fluorescence enhancement factor for molecules with a quantum efficiency of 2.5% and the grey dashed line that for molecules with a quantum efficiency of 100%. **c–e**, Illustration of the simulated structure (side view, section through the two triangle tips) showing regions of fluorescence (**c**, blue), radiative (**d**, red) and non-radiative (**e**, green) enhancement factors for a molecule emitting at a wavelength of 820 nm.

not known, it is highly likely that the molecule is located near the position of maximum field enhancement, that is, between the two triangle tips, as discussed further below. The fluorescence enhancement factor f_F for this SM was determined with the following formula:

$$f_F = (S_{bowtie} P_{un})/(S_{un,max} P_{bowtie})$$

where S_{bowtie} and P_{bowtie} are the SM fluorescence signal and laser excitation power used for Fig. 2b, and $S_{un,max}$ and P_{un} apply to Fig. 2a. At later times, a different single molecule could often be observed to photobleach, enabling measurement of its f_F factor, and so on. In effect, the single molecules randomly sample the possible enhancements that can occur for various positions and orientations near the bowtie.

As is well known, local field enhancement is highly dependent on bowtie gap size. A variety of bowtie sizes were investigated in arrays consisting of 49 bowties or single triangles with the same electron-beam lithography pattern. Confocal scans were taken of each antenna array and the five brightest spots in any array measured as a function of time to look for highly enhanced molecules as determined by significant single photobleaching steps. The gap sizes were then measured by scanning electron microscopy (SEM). Figure 2e is a plot of f_F for 129 SMs measured as a function of bowtie gap size. The bowties with smallest gaps yielded the highest f_F values, up to a factor of 1,340, consistent with bowties with smaller gaps having higher local field strengths than larger-gap bowties and single triangles. Of course, a broader distribution of f_F values occurs because not all molecules are optimally located.

We simulated the nanoantenna by solving Maxwell's equations using the three-dimensional finite-difference time-domain (FDTD) method. The refractive indexes of gold and titanium were modelled by a fit to tabulated experimental data[27] using the method of complex-conjugate pole–residue pairs[28].

To simulate the excitation process, plane waves polarized in the x-direction were incident from the SiO_2 side. The optical intensity enhancement factor driving the increased absorption rate f_E was then obtained by comparing the electric field intensities with and without the metallic bowtie. Figure 3a shows the spectrum of f_E at the centre of the antenna gap region (10 nm above the indium tin oxide (ITO) layer). At a wavelength of 780 nm, the enhancement f_E was 181 in the centre of the bowtie gap, and the maximum field enhancement occurs at the two gold tips (Fig. 1d).

To simulate the emission process, we placed a point current source in the gap region. In the presence of the bowtie antenna, the radiated power P_r into the far field and the power dissipated in the metal P_{nr} were calculated. The enhancement factors were then obtained by normalization with respect to the radiated power

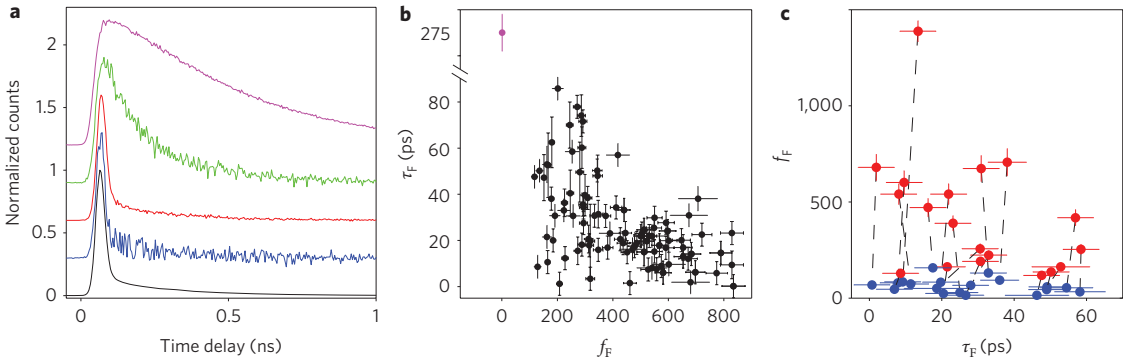

Figure 4 | Fluorescence decay lifetime measurements of single fluorescent molecules (SMs) enhanced by bowtie nanoantennas. a, Time delay histograms. Magenta, bulk TPQDI in PMMA without bowtie nanoantenna; green, SM on bowtie nanoantenna, $f_F = 271$, lifetime 78 ps; red/blue, SM on bowtie nanoantenna, excitation polarization parallel/perpendicular to the long axis; black, instrument response function. **b**, Scatter plot (black points) of decay lifetime versus brightness enhancement for 73 SMs of TPQDI on bowtie nanoantennas. The magenta point indicates bulk TPQDI lifetime without bowtie nanoantenna. **c**, SM TPQDI excited with light polarized parallel/perpendicular (red/blue) to the long axis of the bowtie. The black dashed lines connect measurements from the same molecule. See Methods for an explanation of the error bars.

P_0 of the same point current source in the absence of the antenna. As a result, for a point current source polarized in the x-direction at the centre of the gap emitting at 820 nm, the radiative factor was $f_r \equiv P_r/P_0 = 187$ and the non-radiative factor $f_{nr} \equiv P_{nr}/P_0 = 577$ (Fig. 3d,e). In the vicinity of the antenna, the non-radiative process due to metal loss thus dominates the radiative process, resulting in a quantum efficiency $P_r/(P_r + P_{nr})$ of ~25%.

Based on the simulations above it is possible to estimate the fluorescence enhancement factor. The unenhanced molecule has a low intrinsic fluorescence quantum efficiency of $\eta_0 = [k_{rad,0}/(k_{rad,0} + k_{nonrad,0})] = 2.5\%$, because its intrinsic non-radiative decay rate $k_{nonrad,0}$ dominates over its intrinsic radiative decay rate $k_{rad,0}$. The presence of the antenna should enhance the quantum efficiency by a factor $f_\eta = f_r/[(1 - \eta_0) + \eta_0(f_r + f_{nr})] = 9.32$, which, when multiplied by the field enhancement factor to account for the improved excitation ($f_E = 181$) as calculated above, yields a total fluorescence enhancement ratio $f_F = f_E f_\eta = 1{,}690$. This number is in good agreement with the maximum experimentally measured enhancement factor of 1,340, particularly if one takes into account the experimental uncertainty in determining the exact location and orientation of the molecule. Figure 3b–e shows the enhancement factors at different positions. In the vertical direction (z-direction), the functions are relatively constant in the gap region and fall off quickly above the metal surface (Fig. 3b). In the gap region, the maximum fluorescence enhancement occurs at the centre (Fig. 3c), and falls closer to the metal tip because of lower quantum efficiencies arising from increased ohmic losses (Fig. 3d, radiative; Fig. 3e, non-radiative). The same analysis indicates that a molecule with a high intrinsic quantum efficiency (for example, $\eta > 25\%$) in fact would not have any quantum efficiency enhancement by the same antenna and thus would have a much lower f_F (blue versus grey dashed lines in Fig. 3b; for further discussion see the Supplementary Information).

The discussions above suggest that the enhancement of quantum efficiency should also produce a change in SM total decay lifetime, τ_F. Lifetime changes for ensembles of molecules coupled to plasmonic structures have been reported previously[16]. To investigate this for our SMs, a mode-locked Ti:Sapphire laser tuned to 780 nm was used in conjunction with a fast time resolution APD (Micro Photon Devices (MPD) PDM series) and a time-correlated single-photon counting analyser (Picoharp 300) to measure total decay lifetime. The τ_F value for TPQDI in PMMA in the absence of the antenna is 275 ps (Fig. 4a). To measure τ_F for a SM on a bowtie despite the presence of background fluorescence from other molecules, all fluorescence photons from the molecule-coated bowtie were time-tagged. Time delay histograms could then be formed for the fluorescence photons before and after a SM photobleaching step. The difference in shape of these two time delay histograms is the SM's time delay histogram. Deconvolution of the measured instrument response function (IRF) allowed measurement of lifetimes down to 10 ps. Figure 4a shows a time delay histogram from many molecules away from the bowtie nanoantenna (magenta) as well as from SMs on the bowtie nanoantenna (green and red). SM TPQDI lifetimes shorter than 10 ps were measured on enhanced bowties, a factor of >28 decrease in τ_F.

Compared to measurements of f_F, changes in τ_F only monitor changes in non-radiative and radiative processes and not changes in absorption. Figure 4b presents a scatter plot of SM decay lifetime versus f_F for 73 molecules. At low f_F, both slow and fast τ_F were observed in the data. This result is expected because τ_F depends only upon the radiative and non-radiative rates, but f_F depends also on local intensity, and many combinations are possible for different molecule positions and orientations. To achieve high values of f_F, the molecule's absorption and quantum efficiency must be significantly improved, and this occurs only in the gap where both the radiative and non-radiative rates are larger. Therefore, only short lifetimes are to be expected for high-f_F molecules, as is observed in Fig. 4b.

Because the absorption and emission enhancements are decoupled, the polarization of the excitation light should affect the brightness enhancement but not the SM decay lifetime. An electro-optic polarization rotator was used to cycle the excitation light's linear polarization every 1.5 s, aligning it along either the long or short axis of the bowtie. The fluorescence lifetime as well as f_F for these two polarizations can then be measured for one SM. In Fig. 4a, the red and blue curves represent the SM time delay histograms for long and short axis excitation polarization, respectively, yielding f_F values of 854 and 68, both curves fitting to lifetimes shorter than the IRF. Figure 4c shows the same measurement for 20 more single molecules. The red symbols represent long axis excitation polarization, blue indicating short axis excitation polarization. f_F was measured to change by up to a factor of 16 with different excitation polarization directions, but the lifetime did not change, verifying our general interpretation.

In this work, single molecules of TPQDI were used as probes of f_F near gold bowtie nanoantennas. Using the dominant emission that arises from the most highly enhanced molecule, fluorescence brightness enhancements of up to 1,340 were observed, in agreement with electromagnetic calculations of radiative, non-radiative and electromagnetic intensity enhancements. SM lifetimes show additional

information about the decay processes for each molecule, independent of the local optical intensity enhancement. The bowtie nanoantenna provides a useful balance between enhancement and losses for SM emission applications. In particular, emission decay times as short as 10 ps were observed, which means that a high-emission-rate, room-temperature, single-photon source[29] can be fabricated using a SM in a bowtie gap.

Methods

Bowtie nanoantennas were fabricated using electron-beam lithography (Raith 150) onto 50-nm-thick ITO-coated quartz coverslips. The NIR fluorescent dye TPQDI (for synthesis date see the Supplementary Information) was doped into 1% wt/vol of 75,000 M_W PMMA (Polysciences) in distilled toluene and spun onto the bowtie sample at 2,500 rpm to achieve a final thickness of 30 nm. The sample was imaged using an inverted confocal microscope[9] and the signal collected using a silicon photon-counting APD (Perkin Elmer and MPD). Continuous-wave measurements of fluorescence brightness enhancement were performed with a 780-nm diode laser, and pulsed measurements of fluorescence lifetime used a mode-locked Ti:Sapphire laser (coherent).

Error bars on the bowtie gap size in Fig. 2e were taken to be 1 pixel in the SEM image, where 1 pixel = 1.6 nm. Error bars on f_F (1 s.d.) in Fig. 4b were dominated by the error in determining the brightness of an unenhanced molecule. The standard deviation of the brightness of five unenhanced molecules was found to be 5% and this number was used for error bars in the figure. Finally, error bars (1 s.d.) for the lifetime (Fig. 4c) were found by bootstrapping the fitting parameter.

Received 20 May 2009; accepted 9 September 2009; published online 18 October 2009

References

1. Chance, R. R., Prock, A. & Silbey, R. J. Molecular fluorescence and energy transfer near interfaces. *Adv. Chem. Phys.* **37,** 1–65 (1978).
2. Muhlschlegel, P., Eisler, H., Martin, O. J. F., Hecht, B. & Pohl, D. W. Resonant optical antennas. *Science* **308,** 1607–1609 (2005).
3. Fischer, H. & Martin, O. J. P. Engineering the optical reponse of plasmonic nanoantennas. *Opt. Express* **16,** 9144–9154 (2008).
4. Grober, R. D., Schoelkopf, R. J. & Prober, D. Optical antenna: towards a unity efficiency near-field optical probe. *Appl. Phys. Lett.* **70,** 1354–1356 (1997).
5. Willets, K. A. & Van Duyne, R. P. Localized surface plasmon resonance spectroscopy and sensing. *Annu. Rev. Phys. Chem.* **58,** 267–297 (2007).
6. Hamann, H. F., Kuno, M., Gallagher, A. & Nesbitt, D. J. Molecular fluorescence in the vicinity of a nanoscopic probe. *J. Chem. Phys.* **114,** 8596–8609 (2001).
7. Anger, P., Bharadwaj, P. & Novotny, L. Enhancement and quenching of single-molecule fluorescence. *Phys. Rev. Lett.* **96,** 113002 (2006).
8. Kuhn, S., Hakanson, U., Rogobete, L. & Sandoghdar, V. Enhancement of single-molecule fluorescence using a gold nanoparticle as an optical nanoantenna. *Phys. Rev. Lett.* **97,** 017402 (2006).
9. Schuck, P. J., Fromm, D. P., Sundaramurthy, A., Kino, G. S. & Moerner, W. E. Improving the mismatch between light and nanoscale objects with gold bowtie nanoantennas. *Phys. Rev. Lett.* **94,** 017402 (2005).
10. Farahani, J. N., Pohl, D. W., Eisler, H. & Hecht, B. Single quantum dot coupled to a scanning optical antenna: a tunable superemitter. *Phys. Rev. Lett.* **95,** 017402 (2005).
11. Farahani, J. N. *et al.* Bow-tie optical antenna probes for single-emitter scanning near-field optical microscopy. *Nanotechnology* **18,** 125506 (2007).
12. Tam, F., Goodrich, G. P., Johnson, B. R. & Halas, N. J. Plasmonic enhancement of molecular fluorescence. *Nano Lett.* **7,** 496–501 (2007).
13. Taminiau, T. H., Stefani, F. D., Segerink, F. B. & van Hulst, N. Optical antennas direct single-molecule emission. *Nature Photon.* **2,** 234–237 (2008).
14. Zhang, J., Fu, Y., Chowdhury, M. H. & Lakowicz, J. R. Metal-enhanced single-molecule fluorescence on silver particle monomer and dimer: coupling effect between metal particles. *Nano Lett.* **7,** 2101–2107 (2007).
15. Bakker, R. M. *et al.* Enhanced localized fluorescence in plasmonic nanoantennae. *Appl. Phys. Lett.* **92,** 043101 (2008).
16. Muskens, O. L., Giannini, V., Sanchez-Gil, J. A. & Gomez Rivas, J. Strong enhancement of the radiative decay rate of emitters by single plasmonic nanoantennas. *Nano Lett.* **7,** 2871–2875 (2007).
17. Brolo, A. G. *et al.* Surface plasmon-quantum dot coupling from arrays of nanoholes. *J. Phys. Chem. B* **110,** 8307–8313 (2006).
18. Gerard, D. *et al.* Nanoaperture-enhanced fluorescence: towards higher detection rates with plasmonic metals. *Phys. Rev. B* **77,** 045413 (2008).
19. Ringler, M. *et al.* Shaping emission spectra of fluorescent molecules with single plasmonic nanoresonators. *Phys. Rev. Lett.* **100,** 203002 (2008).
20. Bek, A. *et al.* Fluorescence enhancement in hot spots of AFM-designed gold nanoparticle sandwiches. *Nano Lett.* **8,** 485–490 (2008).
21. Song, J. H., Atay, T., Shi, S. F., Urabe, H. & Nurmikko, A. V. Large enhancement of fluorescence efficiency from CdSe/ZnS quantum dots induced by resonant coupling to spatially controlled surface plasmons. *Nano Lett.* **5,** 1557–1561 (2005).
22. Chen, Y., Munechika, K. & Ginger, D. Dependence of fluorescence intensity on the spectral overlap between fluorophores and plasmon resonant single silver nanoparticles. *Nano Lett.* **7,** 690–696 (2007).
23. Ruppin, R. Decay of an excited molecule near a small metal sphere. *J. Chem. Phys.* **76,** 1681–1683 (1982).
24. Rogobete, L., Kaminski, F., Agio, M. & Sandoghdar, V. Design of plasmonic nanoantennae for enhancing spontaneous emission. *Opt. Lett.* **32,** 1623–1625 (2007).
25. Khurgin, J. B., Sun, G. & Soref, R. A. Practical limits of absorption enhancement near metal nanoparticles. *Appl. Phys. Lett.* **94,** 071103 (2009).
26. Sun, G., Khurgin, J. B. & Soref, R. A. Practical enhancement of photoluminescence by metal nanoparticles. *Appl. Phys. Lett.* **94,** 101103 (2009).
27. Palik, E. D. *Handbook of Optical Constants* (Academic Press, 1985).
28. Han, M., Dutton, R. W. & Fan, S. Model dispersive media in finite-difference time-domain method with complex-conjugate pole–residue pairs. *IEEE Microw. Wireless Comp. Lett.* **16,** 119–121 (2006).
29. Lounis, B. & Moerner, W. E. Single photons on demand from a single molecule at room temperature. *Nature* **407,** 491–493 (2000).
30. Fromm, D. P., Sundaramurthy, A., Schuck, P. J., Kino, G. S. & Moerner, W. E. Gap-dependent optical coupling of single 'bowtie' nanoantennas resonant in the visible. *Nano Lett.* **4,** 957–961 (2004).

Acknowledgements

This work was supported in part by National Science Foundation (NSF) grant DMR-0507296 and by Center for Probing the Nanoscale (CPN) through NSF grant PHY-0425897 (W.E.M.) and by an Air Force Office of Scientific Research (AFOSR) Multidisciplinary University Research Initiative (MURI) program no. FA9550-04-1-0437 (S.F.). Work was performed in part at the Stanford Nanofabrication Facility supported by NSF grant ECS-9731293.

Author contributions

A.K. and W.M. performed experiments and data analysis of experimental data. Z.Y. and S.F. simulated bowtie nanoantennas using FDTD. Y.A. and K.M. synthesized the TPQDI fluorophore.

Additional information

Supplementary information accompanies this paper at www.nature.com/naturephotonics. Reprints and permission information is available online at http://npg.nature.com/reprintsandpermissions/. Correspondence and requests for materials should be addressed to W.E.M.